Optimization on the Tool Parameters in Friction Stir Lap Joining of AA2219 by Response Surface Methodology

B. Babu[a], S.K. Karthikeyan[b], Bachina Harish Babu[c], S. Nanthakumar[d], S. Sakthi[e], P. Vijayalakshmi[f], R. Girimurugan[g], E. Elango[h] and M. Mathanbabu[h]

[a]*Dept. of Agricultural Engg., Indra Ganesan College of Engineering, Trichy, Tamil Nadu, India*
[b]*Dept. of Mech. Engg., Kongunadu College of Engg. and Tech., Tholurpatti, Tamil Nadu, India*
[c]*Dept. of Automobile Engg., VNR Vignana Jyothi Institute of Engg. and Tech., Hyderabad, Telangana, India*
[d]*Dept. of Mech. Engg., PSG Institute of Tech. and Applied Research, Coimbatore, Tamil Nadu, India*
[e]*Dept. of Mech. Engg., Arifa Institute of Tech., Nagapattinam, Tamil Nadu, India*
[f]*Dept. of Mech. Engg., Govt. Polytechnic College, Perundurai, Tamil Nadu, India*
[g]*Dept. of Mech. Engg., Nandha College of Tech., Perundurai, Tamil Nadu, India*
Corresponding Author, Email: dr.r.girimurugan@gmail.com
[h]*Dept. of Mech. Engg., Govt. College of Engg., Krishnagiri, Tamil Nadu, India*

ABSTRACT:

The friction stir welding (FSW) tool's ability to generate heat and strain is crucial to the process's overall performance while performing welding. This study used the RSM to analyse the effects of shoulder diameter, pin diameter and pin height on the temperature, forces and failure load experienced during FSW of AA2219 alloy. There were three components, three stages and seventeen different iterations in this study. A thermocouple was embedded into the samples to measure the welding temperature. In addition, a force measuring device was used to track the amount of pressure applied during the procedure. Using an analysis of variance, it was determined whether or not the resulting model was suitable at 95% confidence level. Through RSM, a correlation was found between tool settings and other input factors and the resulting temperature, force and mechanical qualities of the joints. Afterwards, the optimal processing factors were found by employing a hybrid multi objective optimization based on this connection. According to hybrid multi objective optimization, the best dimensions for a probe are 5.1mm in diameter, 18.43mm in shoulder diameter and 4.12mm in height. Temperature, force and failure load were found to be most affected by shoulder diameter, probe diameter and probe height.

KEYWORDS:

Pin diameter; Shoulder diameter; Temperature; Frictional force; Friction stir welding

CITATION:

B. Babu, S.K. Karthikeyan, B.H. Babu, S. Nanthakumar, S. Sakthi, P. Vijayalakshmi, R. Girimurugan and M. Mathanbabu. 2024. Optimization on the Tool Parameters in Friction Stir Lap Joining of AA2219 by Response Surface Methodology, *Int. J. Vehicle Structures & Systems*, 16(5), 663-670. doi:10.4273/ijvss.16.5.03.

1. Introduction

FSW is a common solid-state welding process used to join aluminium alloys and it was invented by the Welding Institute in 1991 [1]. Since no material melts during the operation, FSW welding minimizes faults caused by melting. Large amounts of frictional heat and plastic deformation are produced by FSW [2, 3]. As a result of both of these factors, the workpiece's internal temperature increased. The temperature history during FSW has a significant impact on the microstructure, including grain size and boundary features and therefore on the mechanical properties of the joints [4-6]. The creation and dispersion of heat during FSW stimulates the microstructural and mechanical properties of the resultant welds [7]. Many studies have looked into how heat and stress affect weld quality during FSW [8-10]. Frictional heat generated at the tool-workpiece interface and plastic deformational heat generated in the weldment

material adjacent to the tool are both factored into a heat production model for FSW of medium-thickness AA 2219 [11, 12]. They investigated how welding factors affected temperature distribution. Maximum temperatures during FSW were predicted by authors using machine learning (ML) methods and regression analysis [13]. A maximum temperature of less than 300°C, an acceptable look, the absence of defects and proper material mixing were all said to be achievable with a tool moving at 1000 rpm [14]. The rotation and traverse movements of the welding tool generate tool welding forces during the FSW process [15, 16].

Determining the force is crucial because an improved comprehension of tool forces allows for better tool development and clamping configurations that lessen tool wear and workpiece distortion [17]. Therefore, it is essential to monitor and manage forces during FSW. The quality of the welded joints and their strength are both enhanced and there are a number of other advantages as well [18]. So far, little research has

been conducted on how to measure these forces and how friction stir welding is affected by them [19]. Using a multivariate empirical model, the authors estimated the vertical force generated by FSW of sheets made of AZ31 [20-22]. The impact of heat generation and strain rate on FSW traversing force has been studied in the literature [23-25]. Researchers combined the outputs of numerical modelling and experimental monitoring to establish a methodology for estimating the traverse force in FSW for different probe profiles [26]. Designing an FSW tool optimal for connecting metals is essential in achieving the desired microstructural and mechanical properties in the resulting joint [27]. The probe with a specified profile and a specific shoulder is the component of the FSW tool, which will be used to determine the joints between the two sheets [28]. After being pressed into the seam between the two samples at high velocity, the shoulder of the tool will contact the material's surface [29]. Moving the tool along the joint line is the next step. Tool probe size, including pin diameter (PD), pin height (PH) and shoulder diameter (SD), significantly affect temperature and force during FSP [30]. The procedure is quite complex, making it challenging to obtain the appropriate FSW parameters. Many academics have been interested in using the RSM method to study and improve various processes, including FSW [31].

The FSW process parameters for aluminium materials were optimized using regression analysis and RSM by the authors [32]. The aluminium type, spindle speed, axial load and tool probe profile were all inputs to FSW. The FSW of AA6061 and TC4 titanium alloys was analyzed using the response surface approach [33]. The RSM technique was used to improve friction stir welding of AA5052-AA6061, as reported in the literature. The results show that increasing the feed rate, rpm rate, or tilt attitude boosts ultimate tensile strength, but only to a certain extent [34]. When it comes to modelling the connection between input and output characteristics, the RSM approach excels [35]. So far, research has been done to check the capability of this model in comparison with other models. For example, authors investigated the model provided by RSM and ANN methods. Their results showed that both methods have a very high capability for modelling [36]. Literatures modelled the process of LaFeO3-NPs for fluoride reduction via the RSM and ANN tools [37-39]. As mentioned, FSW process optimization has been done by researchers with various methods, including RSM. Most of these researches have only investigated the mechanical properties of welding and force and temperature have not been investigated. Also, all these researches are on butt welding and lap welding, which has a different behavior, has not been investigated. For this reason, in this research, using the RSM method, the impact of tool geometry on the force, temperature and tensile strength of the connection are investigated in friction stir lap welding. This study examined how applied force, temperature and tensile strength were impacted using mathematical modelling and statistical analysis. As a method for designing experiments, the RSM was selected. The precision and accuracy of regression equations based on experimental data were evaluated using regression analysis and analysis of variance.

2. Materials and methods

The experiments were carried on plates of AA2219 that were 2.2 mm thick and had the chemical arrangement listed in Table 1. Test equipment is a friction stir welding machine designed to facilitate the FSW method. A revolving spindle is attached to a fixed frame, table and tool head in a horizontally controlled process. To keep a strong grasp on the workpiece and keep track of the axial forces, a specialized device was used. The axial force is detected by two bending load cells and the transverse force is measured by an S-type load cell in this load measuring system. This instrument has a transverse force measurement range of up to 1.5 t with a 5 N resolution and an axial force measurement range of up to 8t with a 15 N resolution, all at the same frequency. FSW was used for the lap joining technique and constant tool speeds of 1000 rpm and 32 mm/min were used. Fig. 1 indicates a simplified diagram of the welding setup. With a precision of 0.1°C, a four-channelled thermometer was used to record the FSW's temperature history. K-type thermocouples were inserted 30mm from the welding line to monitor temperature during FSW. The lap joint was constructed using a variety of H13 steel FSW tools with various SD (D), PD (d) and PH (h). Table 2 includes the dimensions and specifications for welding tools. Peel or shear loading can be used to load lap joints predominantly. In this work, the nominally loaded lap joints in overlap shear were tested for strength. Tensile tests were done to examine the weld's mechanical characteristics. Fig. 2 depicts the dimensions of the test specimens utilized in the lap shear tests.

Table 1: Chemical arrangement of the AA 2219 plates (wt. %)

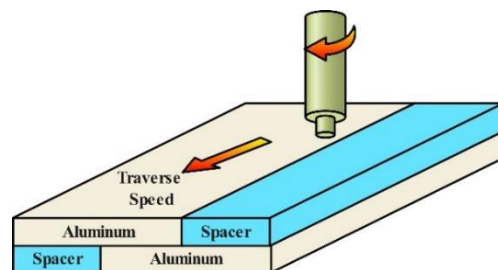| Cu	Mn	Zr	V	Ti	Al
6.3	0.3	0.18	0.10	0.06	Balance

Fig. 1: Schematic presentation of welding setup

Table 2: Input factors and its level in the FSW

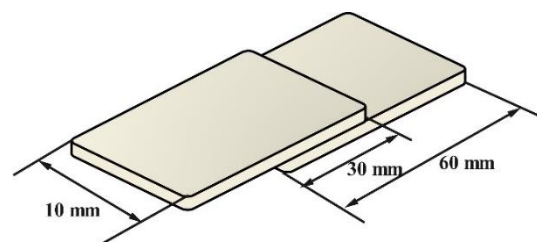| Factors	Symbol	Code	Unit	1	0	1
Shoulder diameter	SD	A	mm	14	18	22
Pin diameter	PD	B	mm	5	7	9
Pin height	PH	C	mm	3	4	5

Fig. 2: An outline of the prepared sample for the tensile shear test

RSM is used to build and enhance models with a response variable that is affected by several independent features. It uses both mathematical and statistical methods. Using a central composite rotatable second-order design (CCD) matrix with star points positioned in the centre of each face of the factorial space, experiments were conducted as per the experimental plan. The numerals 1 and 1 were used to represent the extremes of a component. Using Design Expert software, statistical analysis and experiment design have both been accomplished. Table 3 depicts the design of the FSW experiments. The rows of the design matrix indicate several experiments, while the columns represent the level of tool parameters. The design's central composite component has 17 coded criteria across three tiers and three elements.

Table 3: Layout of the FSW trials

SD (mm)	PD (mm)	PH (mm)	Temperature (°C)	Force (N)	Failure load (kN)
18	7	5.68179	401	7610	1.62
14	5	3	330	4830	3.4
18	7	4	363	6940	2.5
14	9	5	435	11320	2.9
22	9	5	392	6240	3.5
22	5	5	376	7240	2.8
24.7272	7	4	351	5620	4.9
22	9	3	338	3860	3.6
18	3.63641	4	357	5450	4.5
18	10.3636	4	341	4070	2.4
14	5	5	396	7710	4.0
18	7	2.31821	327	4410	1.8
11.2728	7	4	361	5490	4.5
14	9	3	394	7120	1.8
22	5	3	323	3740	2.8
18	7	4	372	6080	5.2
18	7	4	334	4620	1.3

3. Result and discussions

Analysis of variance (ANOVA) was used to test the reliability of the empirical relationship. Tables 4 to 6 show the ANOVA results for the temperature, force and failure load of the joint, respectively. The created model has a substantial F-value for each response. The significance level of a parameter represents its usefulness. The smaller the p value, the greater the importance of a parameter in the model. If the value of 'Prob > F' is less than 0.05, then the model terms are statistically significant. The model is tested using the absence of fit. With a P-value greater than 0.05, it may be concluded that the model adequately fits the data. The proposed model provides a reasonable representation of the overall shape of the data, making the 'lack of fit' test for the response factors irrelevant. When the model term is big and the 'lack of fit' term is modest, however, the analysis is at its best. In a statistical comparison between the model term and the lack of fit term, only the former is shown to be significant. This exemplifies the predictive ability of the fitted model as a result of varying the independent variables. Figs. 3(a-c) show the generated model's prediction performance in comparison to real values. The points on both graphs being so near to the line representing the real number is indicative of a high degree of similarity between the two sets of data. Most problems with RSM include an obscure connection between inputs and outcomes. So, the objective is to get as near as possible to a line of best fit among the group of response factors and the set of independent input components. The FSW's temperature, force and failure load may all be expressed as,

$$Y = f(PD, PH, SD) \qquad (1)$$

Where, PD, PH and SD are independent variables, while Y stands for the response.

Table 4: ANOVA response for the temperature

Source	SSq	df	Mean sq.	F-value	p-value
Model	11957.43	9	1328.60	2.38	0.1329
A-SD	1493.53	1	1493.53	2.68	0.1459
B-PD	839.77	1	839.77	1.50	0.2596
C-PH	8387.74	1	8387.74	15.03	0.0061
AB	648.00	1	648.00	1.16	0.3170
AC	0.0000	1	0.0000	0.0000	1.0000
BC	72.00	1	72.00	0.1290	0.7301
A²	144.66	1	144.66	0.2592	0.6263
B²	13.82	1	13.82	0.0248	0.8794
C²	463.30	1	463.30	0.8301	0.3925
Residual	3907.04	7	558.15		
Lack of fit	3118.37	5	623.67	1.58	0.4309
Pure error	788.67	2	394.33		
Cor. total	15864.47	16			

Table 5: ANOVA response for the force

Source	SSq	df	Mean sq.	F-value	p-value
Model	3.973E+07	9	4.414E+06	1.74	0.2385
A-SD	6.863E+06	1	6.863E+06	2.71	0.1439
B-PD	5.335E+05	1	5.335E+05	0.2104	0.6603
C-PH	2.463E+07	1	2.463E+07	9.72	0.0169
AB	5.746E+06	1	5.746E+06	2.27	0.1759
AC	1.800E+05	1	1.800E+05	0.0710	0.7976
BC	5000.00	1	5000.00	0.0020	0.9658
A²	1.836E+05	1	1.836E+05	0.0724	0.7956
B²	2.655E+05	1	2.655E+05	0.1047	0.7557
C²	9.382E+05	1	9.382E+05	0.3701	0.5622
Residual	1.775E+07	7	2.535E+06		
Lack of fit	1.499E+07	5	2.999E+06	2.18	0.3437
Pure error	2.751E+06	2	1.376E+06		
Cor. total	5.747E+07	16			

Table 6: ANOVA response for the failure load

| Source	SSq	df	Mean sq.	F-value	p-value
Model	13.60	9	1.51	1.16	0.4324
A-SD	0.1186	1	0.1186	0.0910	0.7717
B-PD	1.64	1	1.64	1.26	0.2990
C-PH	0.1232	1	0.1232	0.0946	0.7674
AB	2.20	1	2.20	1.69	0.2345
AC	0.4050	1	0.4050	0.3108	0.5946
Bc	0.0200	1	0.0200	0.0153	0.9049
A²	3.48	1	3.48	2.67	0.1462
B²	0.1460	1	0.1460	0.1120	0.7477
C²	2.83	1	2.83	2.17	0.1838
Residual	9.12	7	1.30		
Lack of fit	1.14	5	0.2285	0.0573	0.9944
Pure error	7.98	2	3.99		
Cor. total	22.72	16			
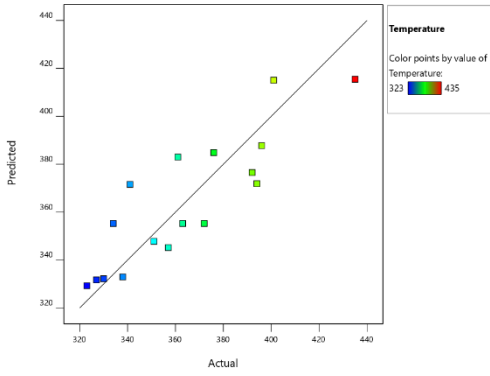
Fig. 3(a): Normal prob. diagram for temperature distribution
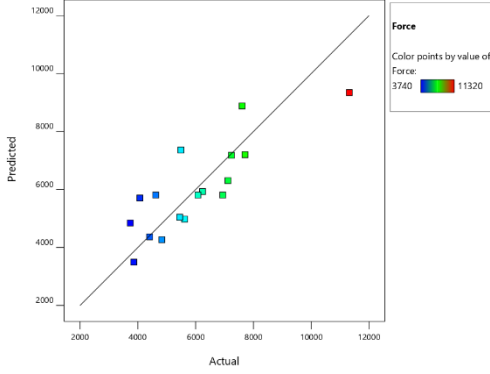

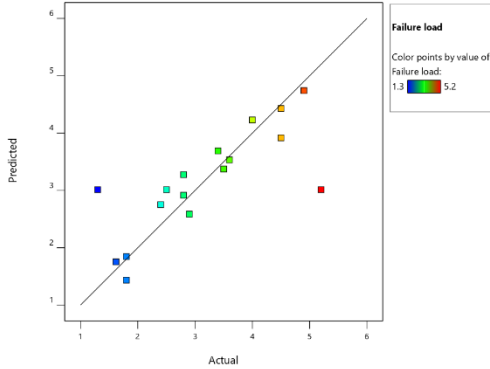**Fig. 3(b): Normal probability diagram for force distribution**

Fig. 3(c): Normal probability diagram for failure load distribution

In this investigation, a second-order model known as the approximation function [38] as below is employed,

$$Y = b_0 + \sum b_i x_i + \sum b_{ii} x_i^2 + \sum b_{ij} x_i x_j + e_r \qquad (2)$$

The offset coefficient is represented by b_0, while the linear, quadratic and variable interaction terms are shown by b_i, b_{ii} and b_{ij} respectively. e_r stands for an unexpected error, whereas x_i and x_j are extra confounding variables. Based on the regression equations obtained from the RSM analysis, predicted values for each response are as follows,

$$\text{Temperature} = 280.66824 - 2.79942\,\text{SD} + 26.29503\,\text{PD} - 16.00265\,\text{PH} - 1.125\,\text{SD} * \text{PD} - 1.36152 \times 10^{-14}\,\text{SD} * \text{PH} - 1.5\,\text{PD} * \text{PH} + 0.223890\,\text{SD}^2 + 0.276840\,\text{PD}^2 + 6.41066\,\text{PH}^2 \qquad (3)$$

$$\text{Force} = -7442.18541 + 427.19551\,\text{SD} + 2492.79211\,\text{PD} - 377.33954\,\text{PH} - 105.9375\,\text{SD} * \text{PD} - 37.5\,\text{SD} * \text{PH} + 7.97615\,\text{SD}^2 - 38.36412\,\text{PD}^2 + 288.48527\,\text{PH}^2 \qquad (4)$$

$$\text{Failure load} = 12.97081 - 1.46149\,\text{SD} - 1.85278\,\text{PD} + 4.94357\,\text{PH} + 0.065625\,\text{SD} * \text{PD} -$$

$$0.056250\,\text{SD} * \text{PH} + 0.025\,\text{PD} * \text{PH} + 0.034734\,\text{SD}^2 + 0.028449\,\text{PD}^2 - 0.501385\,\text{PH}^2 \qquad (5)$$

The temperature history during FSW has a significant impact on the fluid flow and final mechanical qualities. Well-understood methods for connecting materials during FSW processes include frictional heat produced between the FSW tool and the material, softening, mixing and the extruding action of a spinning tool. Friction between the revolving tool and the plate, as well as plastic deformation surrounding the tool, both contribute to the heat produced during FSW. How much heat is generated depends on a number of factors, including how much force is given to the tool, how big the contact area is and how much friction there is between the tool and the workpiece.

Temperature changes can be displayed in either a surface (2D) plot or a contour (3D) plot, depending on the choices made. These response contours may be used to estimate how a specific place inside the design domain would behave. The lowest temperature along the curve of response is the lowest possible. Instead of viewing a series of parallel lines, as is often the case with first-order models, the optimal factor setting for the second-order response may be shown in a contour plot. The temperature of the joint rises as the tool's SD increases, as illustrated in Figs. 4(a-d). Because more of FSW tool and workpiece are in contact, friction heat generation has increased, which is primarily responsible for the temperature rise. Increasing the tool PD, raises the workpiece temperature. Compared to an increase in SD, an increase in PD affects rising temperatures less. This was attributable to the shoulder and workpiece having a broader contact area than the probe and workpiece. Additionally, due to the shoulder's larger radius, its linear velocity is higher than the probe's. It also displays the weld temperature for various PHs. Increasing the PH raises the workpiece's temperature. The primary cause of the temperature increase is an increase in friction heat brought on by an increase in the surface area in contact between the probe side and the material. The temperature response perturbation plot is displayed in Fig. 5. When one tool parameter deviates from the reference point, but all other parameters are held constant at the reference value, the silhouette response and temperature change are shown in this graph. The larger importance of the levels is shown in the ANOVA-obtained F ratio value. According to the F ratio, SD is the most important factor in determining body temperature.
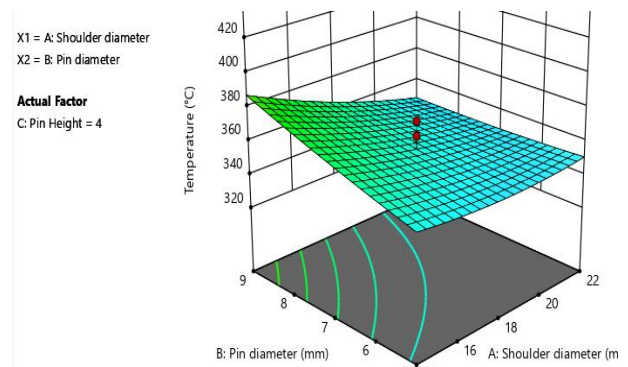

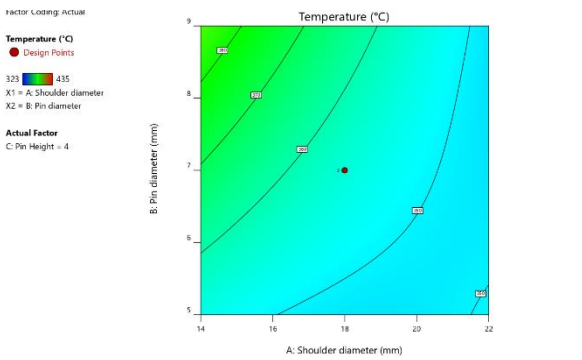**Fig. 4(a): Surface plots of temperature (°C) vs. PD, PH and SD**

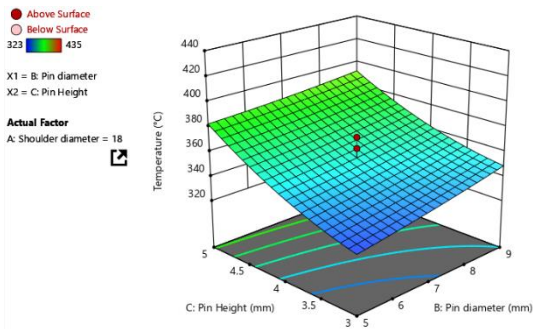**Fig. 4(b): Contour plots of temperature (°C) vs. PD, PH and SD**

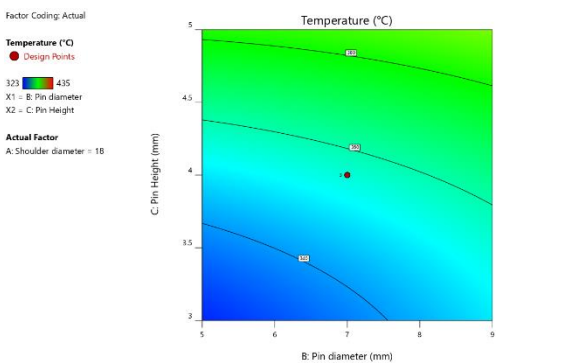**Fig. 4(c): Surface plot of temperature (°C) vs. PD, PH and SD**

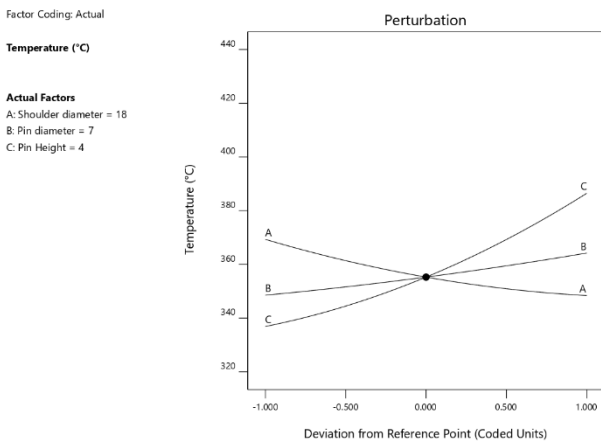**Fig. 4(d): Contour plot of temperature (°C) vs. PD, PH and SD**

Fig. 5: Temperature response of the perturbation plot

The force on the tool rises as the SD grows, although it has less of an impact on the force when compared to the diameter of the tool's pin. This is for the material softens as the SD increases because more heat is created. The extra resistance force resulting from the larger diameter of the tool shoulder is somewhat offset by the more heat generated. The examination of the forces applied to FSW instrument is required for a

number of reasons. First, as the load on the tool grows, its wear rate rapidly rises, resulting in a reduction in tool lifetime and an increase in processing costs. Second, tool wear-related composite impurities may cause the joint to degrade. It would appear vital to ascertain how tool characteristics affect force for this reason. Fig. 6 depicts the evolution of the axial force exerted during the procedure. The samples are initially positioned into a revolving apparatus. During the plunging stage, the axial force significantly rises as a result of the interaction between material softening and work hardening as the tool probe contacts the metal plate. The probe's shoulder contacts the sample's surface after it has first penetrated the workpiece's surface during the plunging phase. The probe penetration zone OA and the shoulder penetration region AB are depicted in Fig. 6 for workpiece and sample surfaces, respectively. When the shoulder fully enters the specimen during the plunge, the axial force is at its maximum. The force is initially rather erratic during the advancing phase, but it steadies and decreases under the peak force experienced through the descending phase after a while. The colder material in front of the tool is not properly churned up at the start of the traverse, which leads to the unstable phase. The plasticized metal under the FSP tool is strain-hardened by the frictional heat created by its rapid rotation. This struggle between increasing heat and increasing work persists until equilibrium is reached.
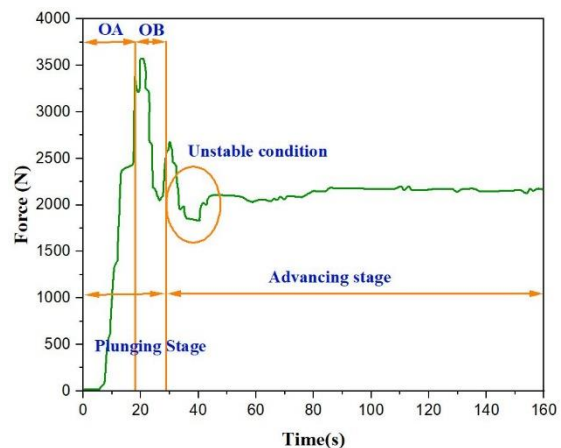

Fig. 6: Axial force history

Figs. 7(a-d) show the average axial force for many FSW tools as 3D surface plots and contour graphs. It may be concluded that increasing the SD causes rising the tool's axial force. The variance in material resistance and heat generation caused by friction in each tool may be the cause of the discrepancy in axial force between tools with various SDs. On the one hand, by enlarging the tool shoulder, more frictional heat is produced, which increases material flow and as a result, softens the workpiece's material, which reduces axial force. However, as the interfacial contact area of the tool grows, so does the material resistance work on the tool. Higher frictional heat and axial forces resulted from the larger SD tool's greater material resistance. Therefore, material resistance has a greater impact on axial force than frictional heat. As the diameter of the probe increases, so does the axial force. That's because more of the probe touched the object being examined. The

resistance force imposed on the tool rises as the probe's diameter grows because a wider area of the material must be sheared and agitated. Axial forces are proportional to the area of the probe that is in contact with the workpiece, therefore increasing the PH has the same effect as increasing the PD. Contour plots and response surface helped us settle on 2489 N as the minimum useful applied force. A tool with a 5mm PD, 3mm PH and 14mm SD will yield this minimal outcome. According to the F ratio, the PD is the single most important factor in achieving a force decrease.
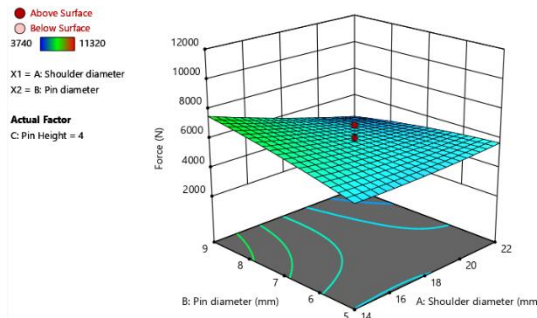
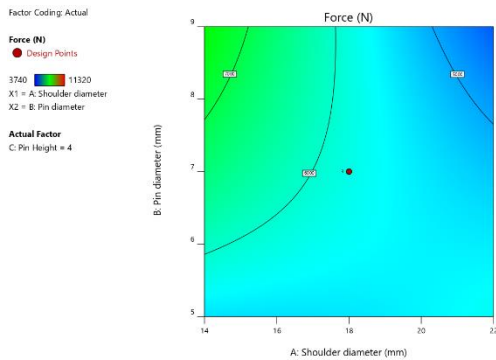**Fig. 7(a): Surface plot of force (N) vs. PD, PH and SD**

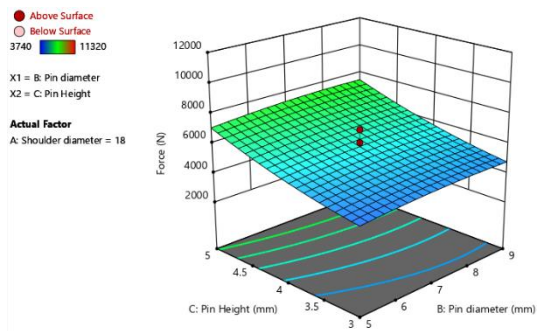**Fig. 7(b): Contour plot of force (N) vs. PD, PH and SD**

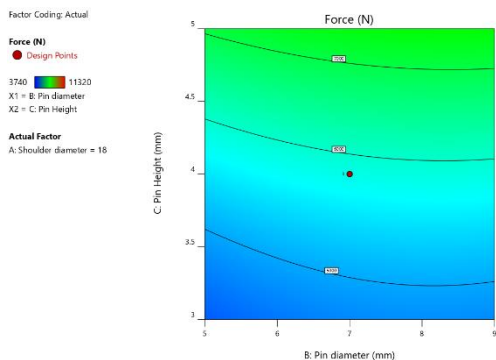**Fig. 7(c): Surface plot of force (N) vs. PD, PH and SD**

Fig. 7(d): Contour plot of force (N) vs. PD, PH and SD

Mechanical properties, such as tensile properties, of FSW joints are known to be highly influenced by probe and SD. The quantity of heat generated during FSW is proportional to the SD of the tool due to friction. Due to an increase in contact area, friction heat output rises as tool SD grows. The surface and contour plots display the failure load of joints for different tool settings in Figs. 8(a-d). Shoulder welds made with 18mm (D/d = 3) sized tools have demonstrated superior tensile characteristics than those formed with 14mm and 22mm (D/d = 1) sized tools, respectively. These outcomes may be explained by the fact that the process produces less heat at lower D/d ratios. This heat generation is unable to create the right environment for improved material mobility. Increasing PH, increases the failure load. This outcome may be explained by the requirement that, in lap welding, the FSW tool probe enters the bottom plate through the top plate to form a strong junction between the two plates.
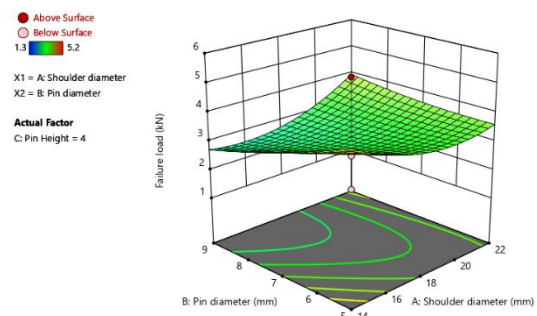

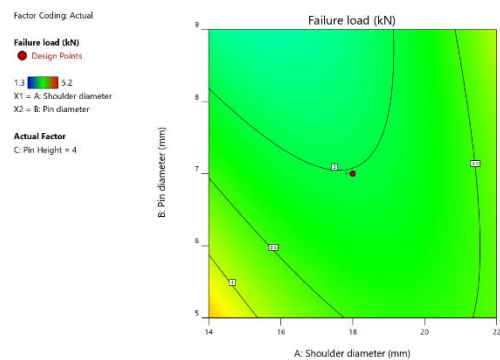**Fig. 8(a): Surface plot of failure load (kN) vs. PD, PH and SD**

Fig. 8(b): Contour plot of failure load (kN) vs. PD, PH and SD
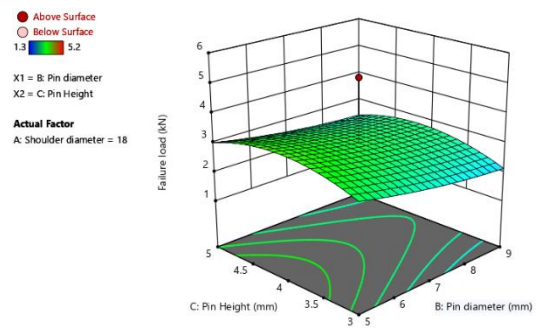

Fig. 8(c): Surface plot of failure load (kN) vs. PD, PH and SD

Increasing the PH improves the bonding areas' interface size and penetration depth into the bottom plate. With PD = 7 mm, SD = 18mm and PH = 5mm, we are able to establish that the highest practical failure load value is 5.1 kN. The failure load value is most sensitive to PH, as indicated by F ratio. When compared to other

parameters, welding is improved by lengthening the pin because it enhances welding depth and material mixing. Increasing the pin length increases the welding depth and the amount of material mixing, which improves the welding compared to other parameters.
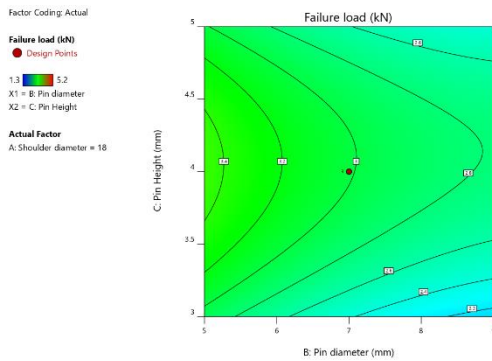

Fig. 8(d): Contour plot of failure load (kN) vs. PD, PH and SD

4. Conclusion

The current study conducted multiple experiments to determine how the critical tool parameters affect the applied force, temperature and failure load in aluminum friction stir lap joining. The PD, PH and SD are the most critical tool parameters and they alter at three separate levels. RSM was used to forecast the responses after the regression model was built. Regression equations were used to model the connections between the inputs and the outcomes. The final step is a hybrid optimization approach to find the optimal process parameters. Weld tensile strength was found to be most affected by tool PH, followed by PD and then SD. By increasing the PH, the welding depth and the amount of material mixing increases, which improves the welding compared to other parameters. The results showed that the force on the tool increases with the increase in the PD and SD, as well as the PH. By increasing the SD, the force on the tool increases, but compared to the PD, it has less effect on the force, which is due to the softening of the material due to more heat produced when the SD increases. This more heat produced partially compensates for the increased resistance force due to the increased SD. Greater tensile characteristics were observed in welds made using 18 mm SD tools (D/d = 3) compared to those made with 14mm and 22mm SD tools. These results could be attributed to the process producing less heat at lower D/d ratios. This heat generation is unable to create the right environment for improved material mobility. With greater D/d ratios, extra heat is produced, which causes a turbulent form of material flow, resulting in poor material mixing and a higher chance that a defect formed in the weld zone. The optimum values are PD of 5 mm, SD of 18 mm and PH of 4 mm.

REFERENCES:

[1] R. Raja, A. Parthiban, S.N. Gopan and D. Degefa. 2022. Investigate the process parameter on the friction stir welding of dissimilar aluminium alloys, *Adv. in Mat. Sci. & Engg.*, 1-8. https://doi.org/10.1155/2022/4980291.

[2] N.Z. Khan, A.N. Siddiquee and Z.A. Khan. 2018. Proposing a new relation for selecting tool pin length in friction stir welding process, *Measurement: J. Int.*

Measure. Confede., 129, 112-118. https://doi.org/10.1016/j.measurement.2018.07.015.

[3] M. Koilraj, V. Sundareswaran, S. Vijayan and S.R.K. Rao. 2012. Friction stir welding of dissimilar aluminum alloys AA2219 to AA5083 - Optimization of process parameters using Taguchi technique, *Mat. & Design*, 42, 1-7. https://doi.org/10.1016/j.matdes.2012.02.016.

[4] R. Manikandan, P. Ponnusamy, S. Nanthakumar, A. Gowrishankar, V. Balambica, R. Girimurugan and S. Mayakannan. 2023. Optimization and experimental investigation on AA6082/WC metal matrix composites by abrasive flow machining process, *Mat. Today: Proc.*, https://doi.org/10.1016/j.matpr.2023.03.274.

[5] B. Rajnaveen, D.B. Naik, G. Rambabu and K.S. Rao. 2022. Optimization of electron beam welding parameters to improve corrosion resistance of AA2219 aluminium alloy, *J. Current Sci. & Tech.*, 12(3), 417-427.

[6] R. Chitwadgi, B. Siddesh, B.L. Shankar, R. Suresh and N.G. Siddeshkumar. 2022. Optimization and analysis of dry sliding wear behaviour of N-B$_4$C/Mos2U reinforced AA2219 nano hybrid composites using response surface methodology, *Metallurgical & Mat. Engg.*, 28(3), 469-485. https://doi.org/10.30544/840.

[7] U. Khalil, M.H. Aziz, S. Qamar and K. Munir. 2023. Parametric optimization on single point incremental forming of aluminum alloy AA 2219-O using response surface methodology, *Arabian J. Sci. & Engg.*, 48(3). 4025-4044. https://doi.org/10.1007/s13369-022-07333-z.

[8] D.B. Naik, C.H.V Rao, K.S. Rao, G.M. Reddy and G. Rambabu. 2022. Optimisation of friction stir welding parameters to improve corrosion resistance and mechanical properties of AA2219 aluminium alloy welds, *Int. J. Comput. Aided Engg. Tech.*, 17(3), 318-334. https://doi.org/10.1504/IJCAET.2022.125714.

[9] B. Babu, S. Meinathan, P. Manikandan, P. Lingeswaran, S. Nanthakumar, A. Yasminebegum and R. Girimurugan. 2023. Investigation on the characterization of hot extruded AA7075 based metal matrix composites developed by powder metallurgy, *J. Physics: Conf. Series*, 2603(1), 012041. https://doi.org/10.1088/1742-6596/2603/1/012041

[10] B. Rajnaveen, G. Rambabu, K. Prakash and K.S. Rao. 2022. A mathematical and experimental approach to improve strength and corrosion resistance of gas tungsten arc, electron beam and friction stir welded AA2219-T87 Al-alloy, *J. Inst. Engg. Series D.*, 104, 1-13. https://doi.org/10.1007/s40033-022-00368-4.

[11] D.B. Naik, C.H.V. Rao, K.S. Rao, G.M. Reddy and G. Rambabu. 2019. Optimization of friction stir welding parameters to improve corrosion resistance and hardness of AA2219 aluminum alloy welds, *Mat. Today Proc,* 15, 76-83. https://doi.org/10.1016/j.matpr.2019.05.027.

[12] G. Rambabu, D.B. Naik, C.H.V. Rao, K.S. Rao and G.M. Reddy. 2015. Optimization of friction stir welding parameters for improved corrosion resistance of AA2219 aluminum alloy joints, *Def. Tech.*, 11(4), 330-337. https://doi.org/10.1016/j.dt.2015.05.003.

[13] M. Akbari and H.R. Asiabaraki. 2023. Modeling and optimization of tool parameters in friction stir lap joining of aluminum using RSM and NSGA II, *Weld. Int.*, 37(1), 21-33. https://doi.org/10.1080/09507116.2022.2164530.

[14] R. Girimurugan, R. Pugazhenthi, T. Suresh, P. Maheskumar and M. Vairavel. 2021. Prediction of mechanical properties of hybrid aluminium composites, *Materials Today: Proc.*, 39, 712-716. https://doi.org/10.1016/j.matpr.2020.09.302.

[15] K.A. Mohammed, S.K. Hussein and A.H. Khuder. 2020. Joining of aluminium alloy AA6061-T6 to PVC polymer by friction stir lap joining process, *IOP Conf. Series: Mat. Sci. & Engg.*, 881(1), 012066. https://doi.org/10.1088/1757-899X/881/1/012066.

[16] T.P. Saju and R.G. Narayanan. 2020. Dieless friction stir lap joining of AA 5050-H32 with AA 6061-T6 at varying pre-drilled hole diameters, *J. Manufacturing Processes*, 53, 21-33. https://doi.org/10.1016/j.jmapro.2020.01.048.

[17] S. Chen, J. Zhang, D. Wang, J. Wang and R. Li. 2019. Study on low axial load friction stir lap joining of 6061-T6 and zinc-coated steel, *Metallurgical & Mat. Trans. A: Physical Metallurgy & Mat. Sci.*, 50(10), 4642-4651. https://doi.org/10.1007/s11661-019-05369-9.

[18] H.S. Bang, A. Das and S. Lee. 2018. Friction stir lap joining of automotive aluminium alloy and carbon-fiber-reinforced plastic, *IOP Conf. Series: Mat. Sci. & Engg.*, 369(1), 012033. https://doi.org/10.1088/1757-899X/369/1/012033.

[19] H.A. Derazkola, F. Khodabakhshi and A. Simchi. 2018. Friction-stir lap-joining of aluminium-magnesium/ poly-methyl-methacrylate hybrid structures: Thermo-mechanical modelling and experimental feasibility study, *Sci. & Tech. of Welding & Joining*, 23(1), 35-49. https://doi.org/10.1080/13621718.2017.1323441.

[20] R. Jayaraman, R. Girimurugan, T. Sankaramoorthy, R. Subbiah and S. Kavitha. 2023. A process of interpreting the performance of friction stir welding on two dissimilar materials, *AIP Conf. Proc.*, 2521(1), 020012. https://doi.org/10.1063/5.0116246.

[21] S. Surendran, T. Sundaram and P. Sathishkumar. 2022. Optimization of surface roughness and tool wear during machining of AMMC using Taguchi technique, *Chiang Mai J. Sci.*, 49(6), 1653-1662. https://doi.org/10.12982/CMJS.2022.095.

[22] M. Shunmugasundaram, A.P. Kumar and D. Maneiah. 2019. An experimental analysis and process parameter optimization on friction stir welded dissimilar alloys, *Int. J. Mech. & Produc. Engg. Res. & Deve.*, 9(2), 407-414. https://doi.org/10.24247/ijmperdapr201939.

[23] S. Vinoth, C. Rajasekar, P. Sathish, V. Sureshkumar, A. Yasminebegum, Sk.H. Ahammad and R. Girimurugan. 2023. Optimization of process parameters on wire cut electrical discharge machining and surface integrity studies of AA6070/MgO composites, *J. Physics: Conf. Series*, 2484(1), 012012. https://doi.org/10.1088/1742-6596/2484/1/012012.

[24] H. Shahmiri, M. Movahedi and A.H. Kokabi. 2017. Friction stir lap joining of aluminium alloy to polypropylene sheets, *Sci. & Tech. of Welding & Joining*, 22(2), 120-126. https://doi.org/10.1080/13621718.2016.1204171.

[25] B.T. Gibson, M.C. Ballun, G.E. Cook and A.M. Strauss. 2015. Friction stir lap joining of 2198 aluminum-lithium alloy with weaving and pulsing variants, *J. Manuf. Processes*, 18, 12-22. https://doi.org/10.1016/j.jmapro.2014.12.002.

[26] V.K. Krishnan, J.V. John and R. Girimurugan. 2023. Optimization of drilling parameters in vertical machining centre drilling on magnesium AZ91D alloy under dry condition with Taguchi design, *Materials Today: Proc.* Online. https://doi.org/10.1016/j.matpr.2023.08.121.

[27] C. Bruni, A. D'Orazio and M.El. Mehtedi. 2015. Friction stir lap joining of blanks under different conditions, *Key Engg. Materials*, 651, 1433-1438. https://doi.org/10.4028/www.scientific.net/KEM.651-653.1433.

[28] M.H. Shojaeefard, M. Akbari, M. Tahani and F. Farhani. 2013. Sensitivity analysis of the artificial neural network outputs in friction stir lap joining of aluminum to brass, *Adv. in Mat. Sci. & Engg.*, 1-7. https://doi.org/10.1155/2013/574914.

[29] M. Akbari and R.A. Behnagh. 2012. Dissimilar friction-stir lap joining of 5083 aluminum alloy to CuZn34 brass, *Metallurgical & Mat. Trans. B: Process Metallurgy & Mat. Processing Sci.*, 43(5), 1177-1186. https://doi.org/10.1007/s11663-012-9682-y.

[30] P. Ji, X. Liu, Y. Zhang, L. Hong and Y. Hao. 2021. Refilling friction stir welding of 20mm thick AA2219 and analysis of microstructure and mechanical properties, *Trans. China Welding Institution*, 42(2), 86-91.

[31] D. Vijayan, V.S. Rao and V.S. Anirudh. 2021. Determination of optimum tensile strength of friction stir welded AA2219 aluminum alloys using Taguchi's method, *Proc. Materials*, 7, 489-497. https://doi.org/10.1007/978-981-15-6267-9_56.

[32] N. Rajan, K. Vijaykumar and R. Girimurugan. 2023. Influence of ECM process parameters on SS316 material, *Materials Today: Proc.* Online. https://doi.org/10.1016/j.matpr.2023.09.059.

[33] K.K. Babu, K. Panneerselvam, P. Sathiya, A.N. Haq, S. Sundarrajan, P. Mastanaiah and C.V.S. Murthy. 2018. Corrosion properties of cryorolled AA2219 friction stir welded joints using different tool pin profiles, *Surface Review & Letters*, 25(03), 1850071. https://doi.org/10.1142/S0218625X18500713.

[34] C.V. Rao, G.M. Reddy and K.S. Rao. 2015. Influence of tool pin profile on microstructure and corrosion behaviour of AA2219 Al-Cu alloy friction stir weld nuggets, *Defence Tech.*, 11(3), 197-208. https://doi.org/10.1016/j.dt.2015.04.004.

[35] M. Vairavel, R. Pughazhenthi, R. Girimurugan and S. Vinothkumar. 2020. Effects of wear characterization analysis of the friction stir welded joints in aluminum alloy Al3116-Cu and A384-Cu, *AIP Conf. Proc.*, 2283(1), 020112. https://doi.org/10.1063/5.0025005.

[36] K.K. Babu, K. Panneerselvam, P. Sathiya, A.N. Haq, S. Sundarrajan, P. Mastanaiah and C.S. Murthy. 2017. Experimental investigation on friction stir welding of cryorolled AA2219 aluminum alloy joints, *Surface Review & Letters*, 24(01), 1750001. https://doi.org/10.1142/S0218625X17500019.

[37] J.Q. Li and H.J. Liu. 2013. Effects of welding speed on microstructures and mechanical properties of AA2219-T6 welded by the reverse dual-rotation friction stir welding, *Int. J. Adv. Manufacturing Tech.*, 68(9-12), 2071-2083. https://doi.org/10.1007/s00170-013-4812-5.

[38] J.Q. Li and H.J. Liu. 2013. Effects of tool rotation speed on microstructures and mechanical properties of AA2219-T6 welded by the external non-rotational shoulder assisted friction stir welding, *Mat. & Des.*, 43, 299-306. https://doi.org/10.1016/j.matdes.2012.07.011.

[39] S. Pandipati, S. Palli, S. Dowwluru, R.C. Sharma, N. Sharma, S.K. Sharma and D. Da Fonseca-Soares. 2024. Microstructure and strength comparison for friction stir processing of aluminium alloys and multi-response optimization by Taguchi GRA-PCA based hybrid methods, *Int. J. Vehicle Structures & Systems*, 16(3), 321-328. https://doi.org/10.4273/ijvss.16.3.03.